DOI: 10.1111/mice.13054

RESEARCH ARTICLE

COMPUTER-AIDED CIVIL AND INFRASTRUCTURE ENGINEERING WILEY

On polymorphic uncertainty modeling in shell buckling

Marc Fina[1] | **Werner Wagner**[1] | **Wolfgang Graf**[2]

[1]Institut für Baustatik, Karlsruher Institut für Technologie, Karlsruhe, Germany

[2]Institut für Statik und Dynamik der Tragwerke, Technische Universität Dresden, Dresden, Germany

Correspondence
Marc Fina, Institut für Baustatik, Karlsruher Institut für Technologie, Karlsruhe, 76131, Baden-Württemberg, Germany.
Email: marc.fina@kit.edu

Abstract

Buckling is typically the governing failure mode of thin-walled shells. In particular, geometric and material imperfections have a major influence on the buckling behavior. Small variations of imperfections have large effects on the load-bearing behavior. However, the design of shells is still characterized by a deterministic way of thinking, in which uncertainties have not yet been sufficiently considered. Even in probabilistic approaches, false assumptions are often generated due to the small amount of experimental data. The focus of this paper is an appropriate uncertainty quantification based on the available data. Therefore, the concept of polymorphic uncertainty modeling is presented on axially loaded shells with different types of imperfections. Finally, an idea for a novel design concept for shells based on a fuzzy-valued safety level is introduced. The paper is intended to initiate a rethinking of the methodology for the numerical design of shells with an appropriate uncertainty quantification.

1 | INTRODUCTION

Shell structures are highly demanded structures, for example, in civil and aerospace engineering. They are thin-walled structures with low dead weight and high load-bearing capacity due to their curved shape. Their slim design is the reason that buckling is usually the governing failure mode. Geometric and material imperfections, such as deviations in the geometric shape and thickness of the shell, residual stresses, and variations in boundary conditions and material parameters, have a major influence on the buckling behavior. Already small variations of imperfections have large influences on the load-bearing behavior. This means that the resistance of thin-walled shells in particular is very low. The shape of imperfections is often unknown or only few measurements are available. Therefore, in traditional design concepts, significant design factors a.k.a. knockdown factors (KDFs) have to be applied, see Hilburger (2012). The development of reliable and more economical KDFs is still part of numerous research projects, see, for example, Wagner et al. (2020).

An alternative concept is the representation of spatially varying imperfections with random fields and autocorrelation functions, see, for example, Broggi and Schuëller (2011), Liang et al. (2022), and Schenk and Schuëller (2003). Therefore, a series of assumptions have to be made for the random field, such as homogeneous or nonhomogeneous and Gaussian or non-Gaussian. Furthermore, the required correlation parameters for modeling of imperfections with random fields have a great influence on the scatter of the buckling loads. Lauterbach et al. (2018) have investigated this influence quantitatively. If the assumptions and correlation parameters are determined based on a limited scope of experiments, the solutions of a probabilistic design concept are not reliable. In addition, test

cylinders under laboratory conditions do not correspond to real structures such as a rocket or a silo.

In reality, all data and information are characterized by various types of uncertainty, for example, natural variability, incompleteness (lack of knowledge), and imprecision (measurement errors). These uncertainties have not been sufficiently considered in traditional concepts. The design of shell structures with deterministic models implies precision. Generally, data uncertainties are characterized by two characteristics, aleatoric and epistemic uncertainty. The quantification of these characteristics for engineering problems is discussed in numerous contributions, for example, Beer et al. (2013) and Faes and Moens (2019). Aleatoric uncertainty is the natural variability. This uncertainty characteristic is already simulated in traditional probabilistic design concepts for shells. The cause of epistemic uncertainty is incompleteness and imprecision of the available data. In contrast to aleatoric uncertainty, epistemic uncertainty can be reduced, for example, by testing more shells experimentally in an early design phase or by an improvement of the accuracy of the measurements.

How aleatoric and epistemic uncertainty can be considered simultaneously in a numerical model is an extensively discussed issue in research. There is an accepted opinion that aleatoric uncertainty can be modeled using stochastic models. The main question under discussion is how epistemic uncertainty can be taken into account. Three main procedures are being investigated for this purpose: possibility theory, Bayesian approach, and imprecise probability (Götz, 2017). In possibility theory, fuzzy sets introduced by Zadeh (1965) are used to describe the possibility of the occurrence of an event (Dubois & Prade, 1988). In the Bayesian approach, an a priori probability (aleatoric uncertainty) is determined based on expert knowledge (epistemic uncertainty). With a likelihood function based on measured data and the Bayes theorem, an a posteriori probability function (Bayesian update) is calculated for a random variable. Applications to the Bayesian approach are given, for example, in Wang et al. (2018). The determination of an a priori probability is regarded as critical (Möller & Beer, 2008). Moreover, the uncertainties are mixed, which is a disadvantage for an engineer who wants to know something about the influence of the epistemic component. In contrast, the approach of imprecise probability allows the separation of epistemic and aleatoric uncertainty. Many different methods are classified under this term, for example, probability boxes (Faes et al., 2021) and fuzzy randomness (Möller & Beer, 2004). In this approach, the concept "polymorphic uncertainty modeling" can be categorized. The concept summarizes several uncertainty models such as random, interval, and fuzzy variables, and combinations of them to consider natural variability, incompleteness, and imprecision simultaneously. This allows an uncertainty quantification without generating false assumptions based on the available data (Götz, 2017). The approach of polymorphic uncertainty modeling is introduced by Graf et al. (2014, 2015). Preliminary works are Beer (2002), Möller et al. (2000), Pannier et al. (2013), and Reuter (2013). The benefits of the approach have already been demonstrated on many engineering tasks. Different uncertainty characteristics for highly scattering material properties of wood are considered with polymorphic uncertainty models in Schietzold et al. (2021). In Freitag et al. (2018), uncertainties of a crack propagation in a reinforced concrete bridge are quantified with the concept of polymorphic uncertainty modeling. In Weber et al. (2019) and Javidan and Kim (2022), the seismic performance of buildings is analyzed with different uncertainty models. Uncertainty characteristics also have to be described in modeling of spatially correlated parameters, where underlying distributions and autocorrelation functions require an appropriate uncertainty quantification. For this purpose, polymorphic uncertainty models are applied to multivariate random fields, see, for example, in Schietzold et al. (2019).

A correlation model with uncertain parameters to simulate surface imperfections of cylindrical shells is presented in Fina et al. (2019b, 2019a) and Fina (2020). The required correlation parameters are evaluated from measurements. There are only a few measurements available, hence the epistemic uncertainty is considered by the definition of the correlation parameters as fuzzy variables leading to a representation of surface imperfections as fuzzy probability–based random fields (fp-rf). Further studies on the correlation model and a sensitivity analysis are given in Fina et al. (2020, 2021). In the mentioned papers, only an uncertainty quantification of surface imperfections for cylindrical shells is presented. The computational novelty of this paper is the introduction of a comprehensive uncertainty quantification for surface, material, boundary, and thickness imperfections based on experimental (limited) data. This leads to improved predictions of experimental buckling loads and allows to propose an alternative safety concept based on a new formulated "danger of buckling." In addition, an approach to model surface imperfections as uncertain random fields for arbitrary structures is proposed. The concept is demonstrated on an axially loaded cylindrical shell and conical shell with cut-outs of the Ariane-3 launcher. The paper's new aspects and essential features can be summarized as follows:

(1) introduction of the concept of polymorphic uncertainty modeling in shell buckling to show an appropriate uncertainty quantification with experimental (limited) data;

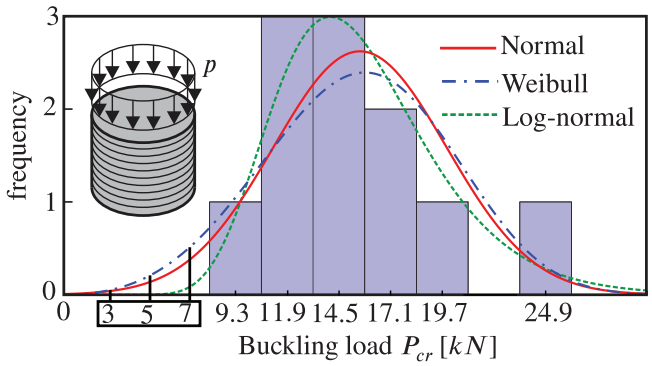

FIGURE 1 Experimental results of $N = 11$ ring stiffened cylindrical shells, the AR-shells from Arbocz and Abramovich (1979): histogram and fitting with three different distribution functions.

(2) uncertainty quantification of different shell imperfections like surface, thickness, boundary, and material imperfections;
(3) approach to simulate surface imperfections as uncertain random fields for arbitrary structures;
(4) proposal of an alternative safety concept based on a new formulated "danger of buckling" considering polymorphic uncertainties.

2 | CONCEPT OF POLYMORPHIC UNCERTAINTY MODELING

The need to introduce the concept of polymorphic uncertainty modeling in shell buckling should be demonstrated with Figure 1. Experimental results of the buckling loads of 11 ring stiffened cylindrical shells from Arbocz and Abramovich (1979) (AR-shells) are presented in a histogram. For all aluminium shells, the Young's modulus and the Possion's ratio are $E = 68,950\,\mathrm{N/mm^2}$ and $\nu = 0.3$. The radius is $R = 101.6$ mm and the average of thickness and length are $t = 0.231$ mm and $L = 136.8$ mm. It is noted that the number of tested shells is very small. This means that epistemic uncertainty can be expected due to the small set of data.

The exceeding probability is to be calculated for a safety assessment. To quantify the natural variability (aleatoric uncertainty), a normal, Weibull, and log-normal distribution are estimated. All three types of distribution are entirely conceivable based on the available small set of data. Table 1 contains the calculated exceeding probabilities for three specified buckling loads that should not be exceeded.

Especially for small exceeding probabilities, that is, in the region of the "tails" of the probability distributions, the deviations of the probabilities are large. This phenomenon

TABLE 1 Exceeding probabilities for different buckling loads assuming normal, Weibull, and log-normal distribution functions.

Distribution	Exceeding probabilities		
	$P_{cr} \le 3\,kN$	$P_{cr} \le 5\,kN$	$P_{cr} \le 7\,kN$
Normal	$1.80 \cdot 10^{-3}$	$7.40 \cdot 10^{-3}$	$2.44 \cdot 10^{-2}$
Weibull	$1.40 \cdot 10^{-3}$	$9.70 \cdot 10^{-3}$	$3.40 \cdot 10^{-2}$
Log-normal	$3.55 \cdot 10^{-10}$	$1.26 \cdot 10^{-5}$	$0.17 \cdot 10^{-2}$

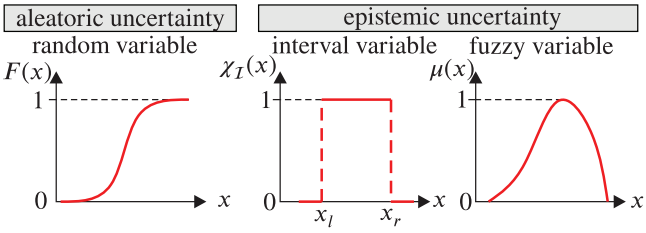

FIGURE 2 Basic uncertainty models: Distribution function of a random variable (left), and interval and fuzzy variable (right).

is also called "tail-sensitivity" problem and has been discussed since the late 1960s, see, for example, Ditlevsen (1982). The safety of a design is determined entirely by the choice of possible distribution functions and associated distribution parameters. This illustrates an inherent uncertainty already in the assumption of density functions if not enough data are available. In the concept of polymorphic uncertainty modeling, developed by Beer (2002), Graf et al. (2015), Möller et al. (2000), Pannier et al. (2013), and Reuter (2013), several uncertainty models are summarized to consider aleatoric and epistemic uncertainties simultaneously.

2.1 | Basic uncertainty models

The idea of the concept of polymorphic uncertainty modeling is to describe both types of uncertainty characteristics with the combination of basic uncertainty models such as random, interval, and fuzzy variables. In Figure 2, the named three basic uncertainty models are depicted.

Random variables are used to describe aleatoric uncertainty. Distribution functions $F(x)$ and density functions $f(x)$ are used to specify a probability measure. The definitions

$$F(x) = F(x, \lambda_X) \quad \text{and} \quad f(x) = f(x, \lambda_X) \tag{1}$$

are intended to show that the associated functions $F(x)$ and $f(x)$ of a random variable are specified by the parameters λ_X, for example, the mean value or standard deviation, see Schietzold et al. (2019). Epistemic uncertainty can

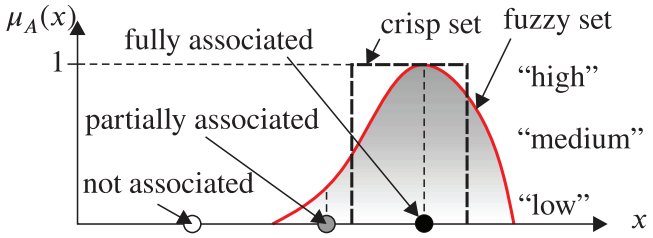

FIGURE 3 Representation of a membership function of an element with a fuzzy and crisp set.

be modeled with interval or fuzzy variables. The theoretical background of fuzzy variables and their numerical treatment is given, for example, in Möller et al. (2000). A normalized fuzzy set $\tilde{A}$ is fully defined as follows

$$\begin{aligned} \tilde{A} &= \{(x, \mu_A(x)) \mid x \in \mathbb{R}\} \\ \mu_A(x) &: \mathbb{R} \to [0,1] \\ \sup_{x \in \mathbb{R}} &[\mu_A(x)] = 1 \end{aligned} \tag{2}$$

where $\mu_A(x)$ is the membership function, that allows to gradually evaluate an element of a set. Thus, elements can assume intermediate states between "fully associated" with $\mu_A(x) = 1$ or "not associated" with $\mu_A(x) = 0$. The value $\mu_A(x) = 1$ is also called trend value and the corresponding element is equivalent to the deterministic case. In Figure 3, the difference between a fuzzy and crisp set is shown.

An evaluation of a membership function is also called "fuzzification" and can be performed based on linguistic assessments and expert knowledge. For this purpose, existing data prepared in a histogram can serve as a reference. Without statistical background, a subjective evaluation of the data is done by making verbal statements about the membership, such as "low," "medium," and "high." The numerical treatment of an uncertainty analysis with fuzzy variables requires the α-discretization, where the membership function is discretized into r α-levels

$$A_{\alpha_k} = \{x \in \mathbb{R} \mid \mu_A(x) \geq \alpha_k\}, \quad k = 1, \ldots, r. \tag{3}$$

In the paper, only convex fuzzy variables are defined. Thus, it follows the short notations of a fuzzy triangular number

$$\tilde{a} = \langle x_\ell, x_m, x_r \rangle \tag{4}$$

An interval is a specific case of a fuzzy variable and can be constructed with $\mu(x_\ell) = 1$ and $\mu(x_r) = 1$ if $x_\ell < x_r$, see Figure 2.

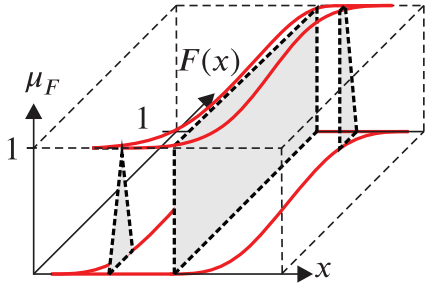

FIGURE 4 Representation of the uncertainty model fuzzy-probability based random variable (fp-r variable).

2.2 | Extension to polymorphic uncertainty models

A combination of the presented basic models leads to new uncertainty models. For example, the combination of a fuzzy and a random variable leads to the model fuzzy probability based random variable (fp-r). A fuzzy-valued probability distribution function results, if at least one distribution parameter λ_X in Equation (1) is defined by a fuzzy variable. Then, the probability space for an fp-r variable is $(\Omega, \Sigma, \hat{P})$. The outcome set of a random event Ω and the Σ-algebra can be taken from the definition of a random variable. The difference to a random variable is that the probability is fuzzy valued. Such a fuzzy-valued probability $\hat{P}$ can be defined as follows:

$$\hat{P} = \left(\hat{P}_\alpha\right)_{\alpha \in (0,1]} \tag{5}$$

where for each $A \in \Sigma$ on a specific α-level, a probability measure is assigned in the form of an interval $\hat{P}_\alpha = [\hat{P}_{\alpha,l}(A), \hat{P}_{\alpha,r}(A)]$. Thus, for each α-level, an associated fuzzy-valued probability distribution function is defined as

$$F_X = \left((F_X)_\alpha\right)_{\alpha \in (0,1]} \tag{6}$$

as depicted in Figure 4. Additionally, in the figure a fuzzy variable is depicted along the $F(x)$-axis, which indicates the fuzzy-valued probability.

Summarizing, an fp-r variable can be described similarly to a random variable by the following mapping:

$$X^{\text{fp-r}} : \Omega \to \mathbb{R} \tag{7}$$

This uncertainty model can be used if not enough data are available to define a distribution function. A particular case of the fp-r variable is the p-box variable or in this terminology the interval probability based random variable (ip-r). This uncertainty model is formed if at least one distribution parameter λ_X in Equation (1) is defined as an interval variable. Then, the probability is interval valued. All such models including the basic uncertainty models

are summarized under the concept of "polymorphic uncertainty modeling." This concept allows to quantify different types of uncertainty without generating false assumptions (Götz, 2017). Moreover, an explicit distinction between aleatoric and epistemic uncertainties is possible.

2.3 | Polymorphic uncertain fields

Some parameters for modeling a structure are variable in space. Examples are the Young's modulus, density, thickness, boundary, and surface variations of a structure. Especially, in shell buckling, the spatial variability of material and geometrical imperfections have to be considered. For modeling aleatoric uncertainty of spatial variability parameters random fields are used. It follows a short summary to random field theory from Vanmarcke (2010) and Sudret and Kiureghian (2000).

A random field $H(\boldsymbol{x},\theta)$ is a scalar field, where for a fixed location $\boldsymbol{x}_0 \in \Omega$, a random variable $H(\boldsymbol{x}_0,\theta)$ is assigned. Thus, a random field can be defined with

$$\{H(\boldsymbol{x},\theta) : \boldsymbol{x} \in \Omega, \theta \in \Theta\} \tag{8}$$

as a collection of random variables. The possible events from the event set Θ of a random experiment are denoted by θ. Furthermore, a realization of a random field for a fixed event θ_0 can be denoted by

$$h_0(\boldsymbol{x}) := H(\boldsymbol{x},\theta_0) \tag{9}$$

For a Gaussian random field, the distribution function at each location is a Gaussian normal distribution with mean $\mu(\boldsymbol{x})$ and variance $\sigma^2(\boldsymbol{x})$:

$$H_0(\theta) := H(\boldsymbol{x}_0,\theta) \sim \mathcal{N}(\mu(\boldsymbol{x}_0),\sigma^2(\boldsymbol{x}_0)) \tag{10}$$

The covariance function containing the second-order information about two locations $\boldsymbol{x}_i$ and $\boldsymbol{x}_j$ is defined as follows:

$$C(\boldsymbol{x}_i,\boldsymbol{x}_j) = E[(H(\boldsymbol{x}_i)-\mu(\boldsymbol{x}_i))(H(\boldsymbol{x}_j)-\mu(\boldsymbol{x}_j))] \tag{11}$$

Normalization by the standard deviations $\sigma(\boldsymbol{x}_i)$ and $\sigma(\boldsymbol{x}_j)$ leads to the autocorrelation function (akf)

$$\rho(\boldsymbol{x}_i,\boldsymbol{x}_j) = \frac{C(\boldsymbol{x}_i,\boldsymbol{x}_j)}{\sigma(\boldsymbol{x}_i)\sigma(\boldsymbol{x}_j)} \tag{12}$$

Alternatively, the akf can be given as a function of the relative distance $\boldsymbol{\tau}$ of two points

$$\rho(\boldsymbol{x}_i,\boldsymbol{x}_j) = \rho(\boldsymbol{\tau}) \quad \text{with} \quad \boldsymbol{\tau} = \boldsymbol{x}_j - \boldsymbol{x}_i \tag{13}$$

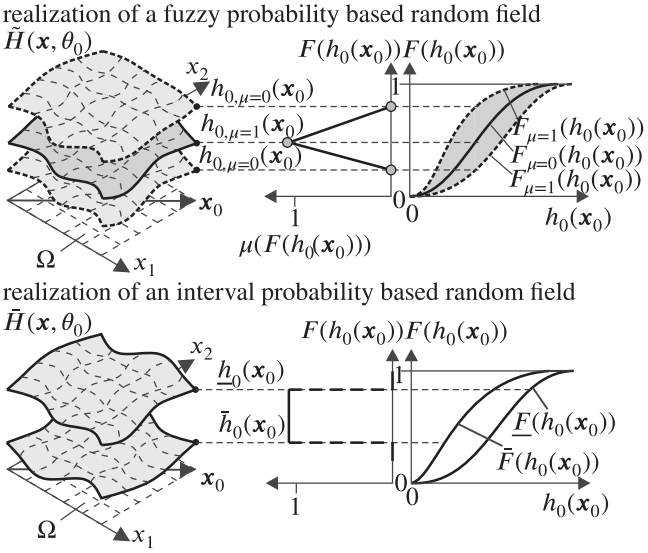

FIGURE 5 Representation of a fuzzy- and interval probability–based random field.

This leads to the homogeneous covariance function

$$C(\tau) = \sigma^2\rho(\boldsymbol{\tau}) \tag{14}$$

A random field is called weakly homogeneous when the first two moments (expected value and variance) in the domain Ω are constant (translationally invariant)

$$\mu(\boldsymbol{x}) = \mu \quad \text{and} \quad \sigma^2(\boldsymbol{x}) = \sigma^2 \tag{15}$$

and the akf is depended only on the distance, see Equation (13). However, the parameters for a random field often cannot be determined exactly. To account for epistemic uncertainty in spatial variability, the random field parameters can be defined by polymorphic uncertainty models, for example, with fuzzy-, interval-, or fuzzy (interval) probability based random variables. The result is a "polymorphic uncertain field." For example, an fp-rf is generated, if at least one of these parameters is defined as a fuzzy variable, see Schietzold et al. (2019):

(1) a distribution parameter of the random field in Equation (15),
(2) a correlation parameter $\tilde{\ell}_c$ to control the akf defined in Equation (14)→ $\tilde{\ell}_c : \tilde{C}(\boldsymbol{\tau},\tilde{\ell}_c)$, or
(3) a distance measure $\tilde{\boldsymbol{\tau}} : \tilde{C}(\tilde{\boldsymbol{\tau}},\ell_c)$.

Then, each realization $\tilde{h}_0(\boldsymbol{x})$ for an event $\theta_0 \in \Theta$ is a fuzzy function. Similarly, any uncertainty model can be used to describe the epistemic component of spatial variability. The fp-rf and ip-rf are depicted in Figure 5.

TABLE 2 Overview of polymorphic uncertain fields considering uncertainties of spatially correlated parameters.

Name of the uncertain field	Mathematical description	Data & uncertainty characteristic
Random field (rf)	$H(\boldsymbol{x},\theta)$ $X : \Omega \to \mathbb{R}$	Aleatoric
Interval field (if)	$\tilde{H}(\boldsymbol{x})$ $\chi_I : \mathbb{R} \to \{0,1\}$	Epistemic, nonevaluated field parameters
Fuzzy field (ff)	$\tilde{H}(\boldsymbol{x})$ $\mu_{\tilde{A}}(\boldsymbol{x}) : \mathbb{R} \to [0,1]$	Epistemic, evaluated field parameters
Fuzzy random field (f-rf)	$\tilde{H}(\boldsymbol{x})$ $X : \Omega \to \mathcal{F}(\mathbb{R})$	Aleatoric & epistemic, evaluated field parameters, imprecision
Interval probability–based random field (ip-rf)	$\tilde{H}(\boldsymbol{x},\theta)$ $X : \Omega \to \mathcal{I}(\mathbb{R})$ $P : \Sigma \to [0,1]$	Aleatoric & epistemic, nonevaluated field parameters
Fuzzy probability–based random field (fp-rf)	$\tilde{H}(\boldsymbol{x},\theta)$ $X : \Omega \to \mathbb{R}$ $\hat{P} = \left(\hat{P}_\alpha\right)_{\alpha\in(0,1]}$	Aleatoric & epistemic, evaluated field parameters, incompleteness
Fuzzy probability–based fuzzy random field (fp-f-rf)	$\tilde{H}(\boldsymbol{x},\theta)$ $X : \Omega \to \mathcal{F}(\mathbb{R})$ $\hat{P} = (\hat{P}_\alpha)_{\alpha\in(0,1]}$	Aleatoric & epistemic, evaluated field parameters, incompleteness & imprecision

An ip-rf results if at least one random field parameter is defined as an interval variable. Thus, on each node of the field, a probability box (p-box) is defined with the following mappings:

$$X : \Omega \to \mathcal{I}(\mathbb{R}) \quad \text{and} \quad P : \Sigma \to [0,1], \tag{16}$$

where the set of all interval sets of $\mathbb{R}$ is denoted by $\mathcal{I}(\mathbb{R})$. If the data to a random field parameter are incomplete and in addition imprecise, the uncertainty model fuzzy–probability based fuzzy random field (fp-r-rf) can be used. This model is defined by the following uncertain mapping on each point of the field:

$$\begin{aligned} X &: \Omega \to \mathcal{F}(\mathbb{R}) \\ \hat{P} &= (\hat{P}_\alpha)_{\alpha\in(0,1]} \end{aligned} \tag{17}$$

where the set of all fuzzy sets of $\mathbb{R}$ is denoted by $\mathcal{F}(\mathbb{R})$. An overview of polymorphic uncertain fields is given in Table 2. Based on the available data, a suitable model can be chosen to quantify all kinds of uncertainties of spatially correlated parameters.

A numerical treatment to generate polymorphic uncertain fields requires an efficient discretization technique. In this paper, the EOLE method (Expansion Optimal Linear Estimation) from Li and Kiureghian (1993) is used. This method allows to define a covariance matrix only on a subset of field nodes, the so-called "random field mesh." A covariance matrix can be generated, for example, with the homogeneous correlation function given in Equation (14). The series of the EOLE method represents a random field with only a few random variables by minimizing the variance error and is given by

$$\hat{H}(\boldsymbol{x},\theta) = \mu(\boldsymbol{x}) + \left(\sum_{i=1}^{M} \frac{\xi_i(\theta)}{\sqrt{\lambda_i}}\,\boldsymbol{\varphi}_i(\boldsymbol{x}^S)\right) C(\boldsymbol{x}^S,\boldsymbol{x}) \tag{18}$$

where the vector $\boldsymbol{x}^S = [\boldsymbol{x}_1 \ \ldots \ \boldsymbol{x}_i^S \ \ldots \ \boldsymbol{x}_M^S]$ contains the number of nodal points M of the random field and $\boldsymbol{x} = [\boldsymbol{x}_1 \ \ldots \ \boldsymbol{x}_j \ \ldots \ \boldsymbol{x}_N]$ the number of nodal points N in full space (e.g., FE nodes). Consequently, $C(\boldsymbol{x}^S,\boldsymbol{x})$ is a covariance matrix containing the covariances of random field nodes to FE-nodes. In Equation (18), $\xi_i(\theta)$ is a standard normal distributed random variable. $\boldsymbol{\varphi}_i(\boldsymbol{x}^S)$ and λ_i are the eigenfunctions and eigenvalues of the defined autocovariance function $C(\boldsymbol{x}_i^S,\boldsymbol{x}_j^S)$ formulated on the random field mesh. The expected value $\mu(\boldsymbol{x})$ can be set to zero if the series represents a spatially correlated field of surface imperfections. However, the separation of the coarser random field mesh from the FE mesh allows keeping the eigenvalue problem as small as possible. Therefore, the EOLE method is recommended in particular when performing a numerical structural analysis with polymorphic uncertain fields. There, the eigenvalue problem of the covariance

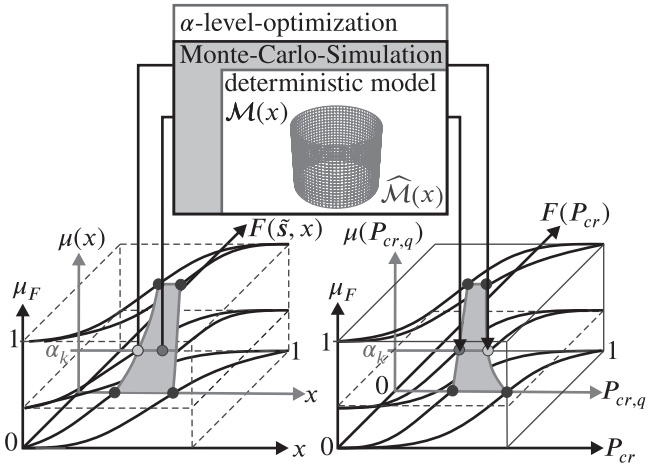

FIGURE 6 Representation of the three-loop computational model for polymorphic uncertainty modeling in shell buckling.

matrix has to be solved several times within a multiloop computational model.

3 | NUMERICAL BUCKLING ANALYSIS WITH POLYMORPHIC UNCERTAIN DATA

The application of polymorphic uncertainty models in shell buckling requires a three-loop computational model, depicted in Figure 6.

The characteristic of the presented computational model is that the outer loop forms the fuzzy analysis with the α-level optimization, which is an optimization strategy based on the α-level discretization, see Equation (3). Therefore, a practical definition of polymorph uncertain input variables is provided by the bunch parameter representation, see, for example, in Möller and Beer (2004). In this representation, epistemic and aleatoric components are decoupled. For example, the fuzziness of the distribution parameters in Equation (15) μ and σ are concentrated in the bunch parameter $\tilde{\boldsymbol{s}} = \{\mu, \sigma, \dots\}$. Thus, a fuzzy cumulative distribution function within an fp-r variable can be simplified as follows:

$$\tilde{F}(x) = F(\tilde{\boldsymbol{s}}, x) \tag{19}$$

A Monte Carlo simulation (middle loop) is performed with a deterministic model (inner loop). In this paper, the deterministic model $\mathcal{M}(\boldsymbol{x})$ represents a finite element (FE) model of axially loaded shells to perform buckling analyses. Consequently, this leads to the representation of the buckling load as an fp-r variable $P_{cr}^{\text{fp-r}}$ as presented in Figure 6. The Monte Carlo simulation (MCS) estimates for a given configuration of bunch parameters $\boldsymbol{s}_0$ the stochastic moments, for example, mean value $\bar{P}_{cr}(\boldsymbol{s} = \boldsymbol{s}_0)$, standard deviation $\sigma_{P_{cr}}(\boldsymbol{s} = \boldsymbol{s}_0)$, or an arbitrary quantile $P_{cr,q}(\boldsymbol{s} = \boldsymbol{s}_0)$. In Figure 6, it is shown that for an arbitrary quantile $P_{cr,q}$ the output quantile values are also fuzzy valued. Considering a specific α-level α_k, the fuzzy bunch parameters are limited by the α-level boundaries

$$\boldsymbol{s} \in \left[\boldsymbol{s}_{\alpha_k,l},\ \boldsymbol{s}_{\alpha_k,r}\right] = \{\boldsymbol{s}_{\alpha_k}\} \tag{20}$$

The corresponding α-level boundaries of the exemplary fuzzy output variable, for example, $P_{cr,q}$, are given by the following extreme value problem:

$$\begin{aligned} P_{cr,q,\alpha_k,l} &= \min_{\boldsymbol{s}\in\{\boldsymbol{s}_{\alpha_k}\}} \left[\mathcal{M}(\boldsymbol{s})\right] \quad \text{and} \\ P_{cr,q,\alpha_k,r} &= \max_{\boldsymbol{s}\in\{\boldsymbol{s}_{\alpha_k}\}} \left[\mathcal{M}(\boldsymbol{s})\right] \end{aligned} \tag{21}$$

where the global extreme values of the stochastic output $\mathcal{M}(\boldsymbol{s})$ in the variable space $\{\boldsymbol{s}_{\alpha_k}\}$ have to be determined. This can be done with an efficient optimization algorithm. However, the solution of these optimization problems can be very time consuming for a complex deterministic model $\mathcal{M}(\boldsymbol{x})$. In order to reduce the computational effort of the α-level optimization, the deterministic model should be replaced with a surrogate model $\widehat{\mathcal{M}}(\boldsymbol{s}) \approx \mathcal{M}(\boldsymbol{s})$. Then the optimization problem in Equation (21) is performed on the previously generated surrogate model $\widehat{\mathcal{M}}(\boldsymbol{s})$. For this purpose, a combined approach of a high-dimensional model representation (HDMR) of second order from Rabitz and Aliş (1999) and least squares (LS) polynomial approximation is used.

In the following chapters, in two examples, an appropriate uncertainty quantification based on limited data is presented. The first example is a conical shell with cutouts of the Ariane-3 launcher. This example is to show the applicability of the approach to real-world problems. The second example is a cylindrical shell, where experimental data are given for surface, boundary, thickness, and material imperfections. To quantify the uncertainties of imperfections, different uncertainty models are presented. This allows to emphasize the advantage of polymorphic uncertainty modeling in shell buckling, that is an uncertainty quantification without generating false assumptions. Both examples are from the aerospace industry. However, the examples should also address civil engineering problems like tanks and silos. In Ditlevsen and Munch-Andersen (1995), correlation functions are presented for a cylindrical concrete silo and in Górski et al. (2015) an aluminium silo is analyzed with random imperfections. The presented methods and algorithms can be applied to such structures if experimental data of imperfections are available. The

presented shells are very thin with a radius-thickness ratio of about $R/t = 101.6\,\text{mm}/0.116\,\text{mm} = 876$. Thus, buckling occurs in the elastic range. However, for civil engineering problems, the R/t-ratios are much smaller. It is noted that the differences between theoretically and experimentally determined critical loads depend on the aspect ratio of the cylinder, in particular are larger for thinner shells, see, for example, Timoshenko and Gere (1961). After a presented appropriate uncertainty quantification, the uncertainties have to propagate through the model by the three-loop algorithm as depicted in Figure 6. A stable and reliable FE model is required. Therefore, a geometric nonlinear quadrilateral shell element with moderate rotations from Wagner and Gruttmann (2005) within an extended version of the general finite element analysis program (FEAP) (Taylor, 2023) is used. The four-node element is based on the isoparametric concept with linear shape functions. Additionally, to avoid shear locking, the assumed natural strain (ANS) method is implemented. To identify a stability point, the diagonal terms of the tangent stiffness matrix are observed. A sign change of a diagonal element indicates a stability point, see, for example, Wagner and Wriggers (1988). Typically for cylindrical shells under axial load a cluster of stability points occurs, which leads to a global failure of the structure. Thus, the postbuckling behavior is not relevant. In case of other structures, for example, stiffened shells or panels, the investigation of the postbuckling regime is mandatory, see, for example, among many others, the example in Gruttmann and Wagner (2006). In the following, the numerical results of the buckling analysis with polymorphic uncertainties are compared with traditional design concepts for both examples. Furthermore, an idea for a novel safety concept based on a formulated fuzzy-valued safety level is presented.

4 | CONICAL SHELL WITH CUT-OUTS OF THE ARIANE LAUNCHER

The model of the Ariane-3 interstage given in Klompé and den Reyer (1989) is depicted in Figure 7.

There are three cut-outs in the shell for the installation of hatches. The isotropic shell is composed of 10 curved aluminum segments. The Young's modulus is $E = 60,000\,\text{N/mm}^2$ and the Poisson's ratio is $\nu = 0{,}34$. Due to the small shell thickness of $t = 1.8\,\text{mm}$, plastic buckling can be excluded. To simulate the experimental buckling test, the shell is simply supported on both edges, where the SS-3 boundary conditions hold at the lower edge: $u = v = w = 0$, $\varphi_x \neq 0, \varphi_y \neq 0$, and the upper edge: $u = \Delta u$,

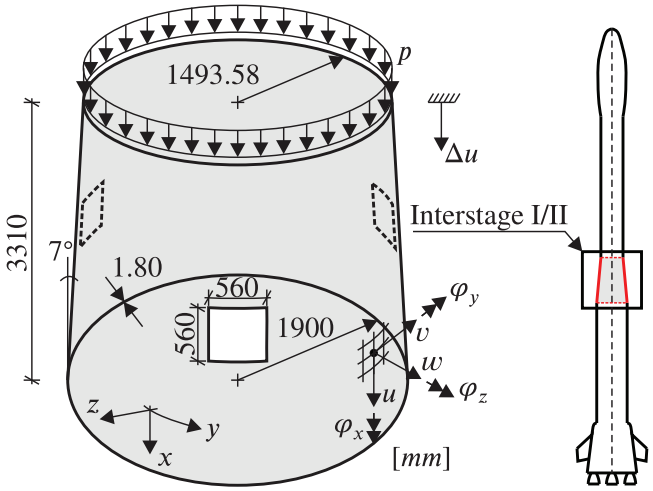

FIGURE 7 Model of the Ariane-3 interstage I/II.

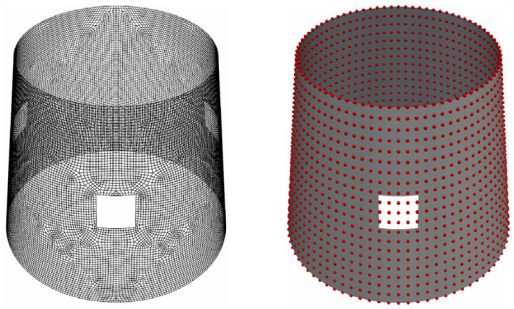

FIGURE 8 FE model of the conical shell: FE mesh with 22, 546 nodes and 22, 032 elements (left) and random field mesh with 81×21 nodes (right).

$v = w = 0, \varphi_x \neq 0, \varphi_y \neq 0$. The axial load is applied using a displacement control Δu until a stability point is reached. An FE mesh with 22, 032 elements and 22, 546 nodes is generated using the mesh generator NeGe from Sienz (1992). Surface imperfections are deviations in radial z-direction and are modeled as fp-rfs. Therefore, the EOLE method according Equation (18) is applied. In contrast to the distorted FE mesh, a uniform random field mesh with 81×21 nodes is defined. Both meshes are depicted in Figure 8.

Assuming that the cut-outs were manufactured after the imperfection measurements, random field nodes are set in the area of the cut-outs (hatches). The choice of the random field mesh can be justified by the manufacturing process. In addition, a smaller number of nodes reduces the computational effort and memory costs solving the eigenvalue problem with the covariance matrix $C(\boldsymbol{x}^S, \boldsymbol{x})$ in Equation (18).

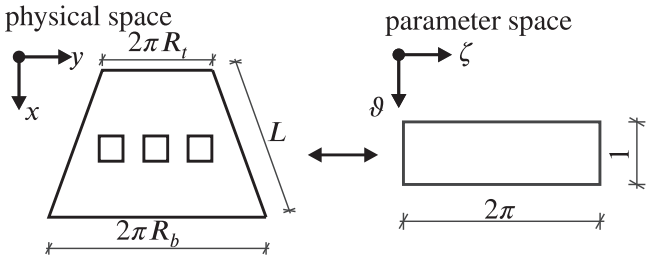

FIGURE 9 Projected area of the conical shell in physical space (left) and parameter space (right).

4.1 | Uncertainty quantification of surface imperfections

In the data bank from Klompé and den Reyer (1989), measurement to surface imperfections of eight original conical shells of the Ariane-3 interstage I/II are documented. With the Fourier coefficients given therein, the imperfections can be represented as Fourier series. Surface imperfections are variations from the ideal shell surface and have a major influence on the buckling load. Particularly in this case, a comprehensive quantification of the uncertainties is very important. The fp-rfs are used to consider aleatoric and epistemic uncertainty of the spatially correlated surface imperfections. Therefore, a correlation model to generate random fields is required. An approach to the evaluation of akfs from given Fourier series for a cylindrical shell without cut-outs is presented in a previous paper, see Fina et al. (2020). In the following, it is shown how the approach can be applied for arbitrary structures. The projected surface of the Ariane interstage is a trapezoid with cut-outs. The distance calculation for generating the akfs can be performed on this projected surface. In addition, the coordinates are transformed from physical space into a parameter space $\vartheta \in [0,1]$ and $\zeta \in [0, 2\pi]$, see Figure 9.

In consideration with the definition of the random field mesh according to Figure 8, the cut-outs in the parameter space are neglected. Thus, the fully separable correlation model

$$C(\Delta\vartheta, \Delta\zeta) = \sigma_n^2 \, \rho_n(\Delta\vartheta) \, \rho_n(\Delta\zeta) \tag{22}$$

is constructed on the parameter space, where $\rho_n(\Delta\vartheta)$ and $\rho_n(\Delta\zeta)$ are the one-dimensional akfs along the axial and circumferential direction with the corresponding lags $\Delta\vartheta$ and $\Delta\zeta$. σ_n^2 is the sample variance. The lags in both directions can be calculated as follows:

$$\boldsymbol{\tau} = \begin{Bmatrix} |\vartheta_i - \vartheta_j| \\ |\zeta_i - \zeta_j| \end{Bmatrix} = \begin{Bmatrix} \Delta\vartheta \\ \Delta\zeta \end{Bmatrix} \tag{23}$$

TABLE 3 Fitting results of the correlation lengths $\ell_{c,h}$, $\ell_{c,u}$ and the variance σ^2.

Shell	1	2	3	4	5	6	7	8
$\tilde{\sigma}^2$ (mm^2)	0.26	0.31	0.26	0.34	0.40	0.43	0.50	0.36
$\ell_{c,h}$ (mm^2)	0.14	0.12	0.10	0.13	0.16	0.12	0.17	0.21
$\ell_{c,u}$ (mm)	3.15	2.09	2.37	1.96	2.12	0.23	2.02	1.88

Further equations and assumptions to calculate both independent akfs are given in Fina et al. (2020). The eight akfs $\rho_n(\Delta\vartheta)$ and $\rho_n(\Delta\zeta)$ vary from shell to shell. The next step is to fit these functions using a nonlinear LS method. The fitting results are correlation lengths as fitting parameters. Therefore, suitable fitting functions based on the parameter space have to be defined. For a fit of the axial akfs, the squared exponential function

$$\rho(\Delta\vartheta, \ell_{c,h}) = \exp\left(-\frac{\Delta\vartheta^2}{\ell_{c,h}}\right) \tag{24}$$

with the correlation length $\ell_{c,h}$ is chosen. Furthermore, the linear-cosine form

$$\rho(\Delta\zeta, \ell_{c,u}, T) = \left(1 - \frac{\Delta\zeta}{\ell_{c,u}}\right) \cdot \cos\left(\frac{2\pi\Delta\zeta}{T}\right) \tag{25}$$

is used for fitting the circumferential akfs, where $\ell_{c,u}$ is the associated correlation length. Since the akfs are defined on the parameter space, the correlation lengths are dimensionless. The period length T is obtained from the fitting as the average of all seven correlation curves and amounts $T \approx \frac{2}{3}\pi$. This parameter has been taken equal for all eight shells in the series to reduce later the number of input variables. The fitting results of the correlation lengths $\ell_{c,h}$, $\ell_{c,u}$ and the variance σ^2 are given in Table 3 and presented in a histogram in Figure 10.

The final step to model surface imperfections as fp-rfs is to transform the akf given in Equation (22) to an akf with polymorphic uncertain parameters

$$\tilde{C}(\boldsymbol{\tau}) = \tilde{\sigma}^2 \, \tilde{\rho}(\Delta\vartheta) \, \tilde{\rho}(\Delta\zeta) \tag{26}$$

where the variance $\tilde{\sigma}^2$ and the correlation parameters $\tilde{\ell}_{c,h}$ in $\rho(\Delta\vartheta)$ and $\tilde{\ell}_{c,u}$ in $\rho(\Delta\zeta)$ are the uncertain parameters. For these parameters, the lack of knowledge due to a small sample size has to be considered. The sample size of eight shells allows to evaluate the data. Thus, fuzzy variables are defined based on the available data. As a first design aid, the membership function is defined based on the histogram in the background. In this case, fuzzy trapezoidal and fuzzy triangular numbers are chosen. The corresponding fuzzy and sample akfs of the eight shells are depicted in Figure 11.

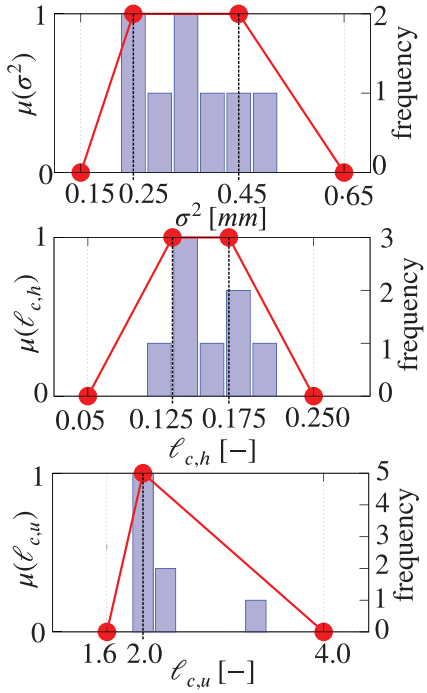

FIGURE 10 Membership functions for the variance and correlation parameters: variance (above), correlation parameter in axial direction (middle), and circumferential direction (below).

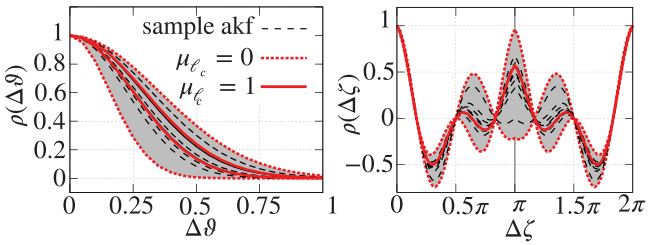

FIGURE 11 Fuzzy and sample akfs in axial (left) and circumferential (right) direction.

The eight sample akfs result from inserting the correlation parameters $\ell_{c,h}$ and $\ell_{c,u}$ from the histogram in Figure 10 into the akfs given in Equation (24) and Equation (25). With the defined fuzzy numbers in Figure 10, the fuzzy functions for $\mu_{\ell_c} = 0$ and $\mu_{\ell_c} = 1$ can be generated. As shown in Figure 11, all akfs are covered by the defined fuzzy functions. Of course, any membership functions with linear or nonlinear branches oriented in the available data are also conceivable. Due to the lack of expert knowledge, all samples lie in the support set with a conservative overhanging of the membership function. The presented fuzzification based on subjective optical examination of the data can lack some kind of consistency when almost no expert knowledge to the parameters is available. It is important that the fuzzification of the parameters can be clearly justified. Finally, two realizations of surface

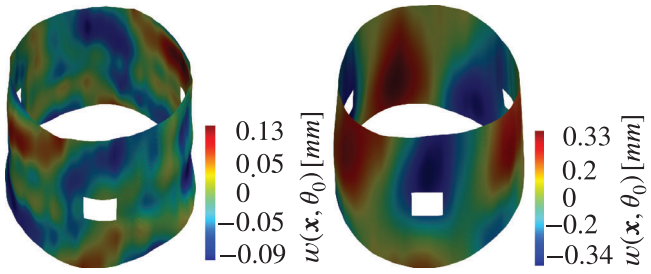

FIGURE 12 Realizations of surface imperfections of the conical shell with cut-outs (100 times enlarged): Fuzzy input parameters $\ell_{c,h} = 0.05$, $\ell_{c,u} = 1.6$, and $\sigma^2 = 0.15$ mm (left) and $\ell_{c,h} = 0.25$, $\ell_{c,u} = 4.0$, and $\sigma^2 = 0.65$ mm (right).

imperfections are depicted in Figure 12. Therefore, the left and right bounds of the fuzzy input parameters $\ell_{c,h}$, $\ell_{c,u}$, and σ^2 from Figure 10 are chosen to simulate the random fields.

4.2 | Numerical results

A nonlinear stability analysis provides the ideal buckling load $P_{\text{cr,perf}} = 248.92$ kN with the corresponding critical displacement $u_{\text{cr,perf}} = 0.92$ mm. An analytical solution for the ideal buckling load of a conical shell under axial pressure with a semivertex angle $\alpha = 7°$ can be calculated as follows, see Weingarten and Seide (1968):

$$P_{\text{cr,perf}} = \frac{2\pi E t^2 \cos^2(\alpha)}{\sqrt{3(1-\nu^2)}} = 738.74\,\text{kN} \tag{27}$$

In comparison, the three cut-outs lead to a large reduction of the stability load: $248.92/738.74 = 0.34$. All buckling loads P_{cr} are normalized by the critical load $P_{cr,\text{perf}} = 248.92$ kN of the perfect shell by

$$\alpha_{cr} = \frac{P_{cr}}{P_{cr,\text{perf}}} \tag{28}$$

where α_{cr} is denoted as the critical buckling load factor. The results of the buckling analysis with the uncertain input parameters $\ell_{c,h}$, $\ell_{c,u}$, and σ^2 are depicted in Figure 13.

The critical buckling load factor is an fp-r variable from which the membership function $\mu(\alpha_{\text{cr},0.05})$ of the fuzzy 5% quantile $\alpha_{\text{cr},0.05}$ is depicted. The α-level optimization is solved based on a second-order HDMR surrogate model with the LS method and cubic polynomials to approximate the cut functions. A sampling on the cut functions leads to 61 sample points for a number of $n_{\text{sim}} = 5$ grid points per variable. On each sample point, an MCS with 500 realizations is performed. It follows a computational effort

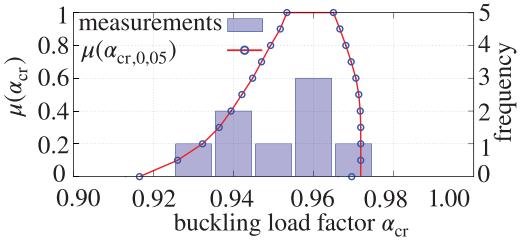

FIGURE 13 Results of the buckling analysis with uncertain parameters of surface imperfections.

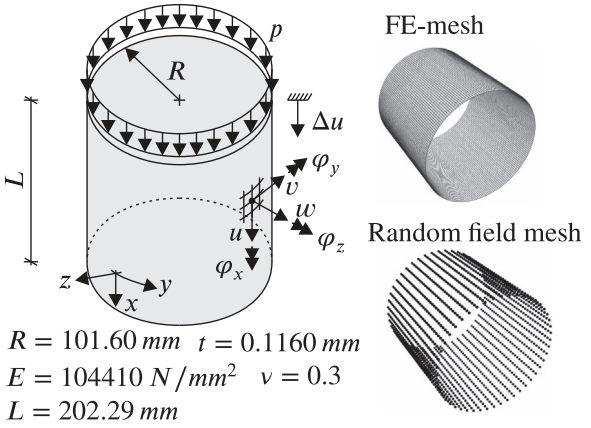

FIGURE 14 Finite element model of the axially loaded cylindrical shell.

with $61 \times 500 = 30,500$ buckling analyses. In addition, the measured imperfections in the form of Fourier series are applied to the FE model. The corresponding results of the critical buckling factor are shown in the histogram in Figure 13. A good agreement of the measurements with the fuzzy 5% quantile value can be shown. This indicates an appropriate uncertainty quantification. The left limit of the fuzzy 5% quantile value is $\alpha_{cr} \approx 0.92$. This small KDF shows that the stability behavior of the conical shell is less sensitive to the existing surface imperfections. Nevertheless, other imperfection forms like material, boundary, and thickness imperfections and their uncertainties should be modeled.

5 | CYLINDRICAL SHELL UNDER AXIAL PRESSURE

On a cylindrical shell under axial pressure, an appropriate uncertainty quantification based on experimental data is presented for all kinds of imperfections like boundary, thickness, material, and surface imperfections. From Delft's imperfection data bank (Arbocz & Abramovich, 1979), a representative shell of the test series "A-shells" is selected, where data for all imperfection types are available. The test series includes only seven shells. This small sample size indicates a high epistemic component of the available data, which has to be appropriately quantified. The FE mesh and random field mesh of the axially loaded cylindrical shell are depicted in Figure 14.

Dimensions and material properties are the averaged values of the seven investigated A-shells from Delft's imperfection data bank from Arbocz and Abramovich (1979). The shell is simply supported on both edges, where the SS-3 boundary conditions hold at the lower edge: $u = v = w = 0$, $\varphi_x \neq 0, \varphi_y \neq 0$, and the upper edge: $u = \Delta u$, $v = w = 0$, $\varphi_x \neq 0, \varphi_y \neq 0$. The cylinder is loaded by displacement control with Δu at the top until the stability point is reached. The FE mesh consists of 200 elements in circumferential direction and 100 elements in axial direction. The surface imperfections are modeled as deviations in radial z-direction. To generate surface imperfections according to Equation (18), a random field mesh is defined with 49×31 points. The total number of points are the number of points that are used for measurements of the surface imperfections given in the data bank.

5.1 | Uncertainty model for surface imperfections

For the presented cylindrical shell, surface imperfections are analyzed in Fina et al. (2020). From this paper, the uncertainty quantification of the three parameters $\ell_{c,h}$, $\ell_{c,u}$, and σ^2 is adopted to simulate an fp-rf. The parameters are given in Table 5. In Fina et al. (2020), the numerical results do not align with the experimental results, as only the uncertainties of surface imperfections are taken into account. The main objective of this research is to demonstrate a comprehensive quantification of uncertainties associated with surface, material, boundary, and thickness imperfections based on limited data, in order to improve the prediction accuracy of experimental buckling loads. Consequently, it follows an extensive discussion on uncertainty quantification for various types of shell imperfections.

5.2 | Uncertainty model for boundary imperfections

Boundary imperfections can lead to a drastic reduction of the buckling load. This kind of imperfections result of the unevenness of the boundaries at the bottom and top of the shell. Only few measurements to this kind of imperfection

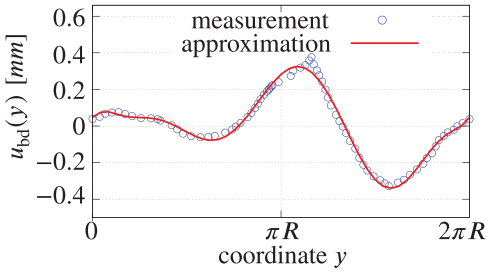

FIGURE 15 Measured boundary imperfection and their approximation.

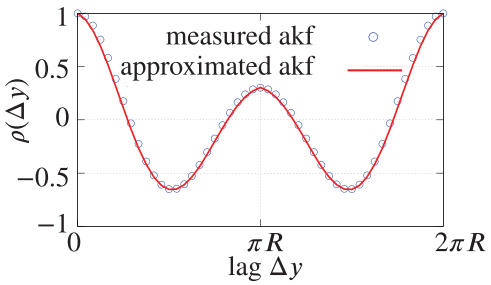

FIGURE 16 Akf of measured boundary imperfection and their approximation.

are available in the literature. However, a model as a one-dimensional ip-rf is possible. Therefore, in Arbocz (2000), a measurement of boundary imperfections around a cylindrical shell with similar dimensions of the investigated A-shells is published. This single measurement allows to estimate the spatial variability of boundary imperfections. The measurement and their approximated function $u_{\mathrm{bd}}(y)$ that is needed for further calculation is shown in Figure 15, where the approximated function is generated by the linear LS method with a polynomial degree of $p = 10$ and $N = 75$ samples.

With equation

$$\rho(\eta\Delta y_0) = \frac{1}{N-1}\sum_{n=1}^{N-1}(u_{\mathrm{bd}}(y_n + \eta\Delta y_0) - \bar{\mu})(u_{\mathrm{bd}}(y_n) - \bar{\mu}) \tag{29}$$

a representative akf in circumferential direction can be calculated. Therein, $u_{\mathrm{bd}}(y_c)$ is the one-dimensional stochastic process representing the boundary imperfection with the sample mean $\bar{\mu}$ and $\eta = 0 \ \ldots \ N_C - 1$ is the number of multiples of a constant distance Δy_0. Similar to the determination of the akfs for the surface imperfections, the linear cosine function

$$\rho(\Delta y, \ell_{c,\mathrm{bd}}, T_{\mathrm{bd}}) = \left(1 - \frac{\Delta y}{\ell_{c,\mathrm{bd}}}\right) \cdot \cos\left(\frac{2\pi\Delta y}{T_{\mathrm{bd}}}\right) \tag{30}$$

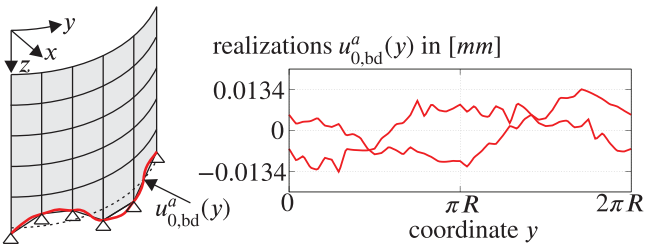

FIGURE 17 Modeling of boundary imperfections in the finite element (FE) model (left) with two realizations of the random field (right).

is used for an approximation. The correlation parameter $\ell_{c,\mathrm{bd}} = 494$ mm and the period length $T_{\mathrm{bd}} = 349$ mm result in a good approximation. The akf and its approximation are depicted in Figure 16.

With the akf, the covariance matrix in the form

$$C(\Delta y) = \sigma^2 \rho(\Delta y, \ell_{c,\mathrm{bd}}, T_{\mathrm{bd}}) \tag{31}$$

can be calculated for a simulation of boundary imperfections as a homogeneous standard normally distributed random field defined as follows:

$$u_{\mathrm{bd}}(\boldsymbol{y}, \theta) \sim \mathcal{N}(0, 1) \tag{32}$$

The only available measurement is a reference to estimate the shape of boundary imperfections. No more detailed information is given about the variance and amplitude. Therefore, realizations of the random field are scaled with an amplitude factor a_{bd} related to the displacement u_{cr} as follows:

$$u^a_{0,\mathrm{bd}}(y_i) = \frac{u_{\mathrm{bd}}(y_i)}{||u_{0,\mathrm{bd}}(\boldsymbol{y})||_{\max}} \cdot \frac{u_{\mathrm{cr}}}{a_{\mathrm{bd}}} \quad \text{with} \quad i = 1 \ldots N \tag{33}$$

The numerically calculated displacement u_{cr} is the associated displacement to the buckling load P_{cr} of the shell without any imperfections. Details to identify a stability point and calculation of buckling loads will be given later in Section 5.5. For the investigated shell, the displacement is $u_{cr} = 0.134$ mm. Figure 17 shows exemplary two realizations of the random field for $a_{\mathrm{bd}} = 10$ mm, $\ell_{c,\mathrm{bd}} = 494$ mm, and $T_{\mathrm{bd}} = 349$ mm.

Furthermore, Figure 17 (left) illustrates the incorporation of boundary imperfections in the FE model. These are applied in the form of support displacements $\boldsymbol{u}$ in the x-direction at the bottom edge of the cylinder. The impressed displacements as realizations of a random field result in a nonuniform stress state in the shell, which is similar to an imperfection.

Based on the available data, an ip-rf is chosen as the suitable uncertainty model. With only one measurement

TABLE 4 Experimental results for Young's modulus E (N/mm^2) and shell thickness t (mm) of the seven A-shells.

	A-7	A-8	A-9	A-10	A-12	A-13	A-14
E	104110	104800	101350	102730	104800	104110	108940
t	0.1140	0.1179	0.1153	0.1204	0.1204	0.1128	0.1110

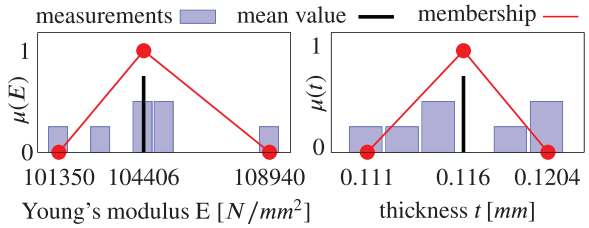

FIGURE 18 Histogram and membership function of Young's modulus E (left) and shell thickness t (right).

for the correlation property, no evaluation of the data is possible and the parameters cannot be defined by fuzzy variables. Therefore, the introduced parameters are defined as intervals

$$T_{\text{bd}} \in [100\,\text{mm},\ 500\,\text{mm}] \quad \text{and} \quad a_{\text{bd}} \in [10\,\text{mm},\ 20\,\text{mm}] \tag{34}$$

A parameter study of the correlation parameter $\ell_{c,\text{bd}}$ has shown that this parameter has no significant influence on the buckling behavior. Thus, the parameter is defined as a deterministic variable: $\ell_{c,\text{bd}} = 494\,\text{mm}$. However, the amplitude factor a_{bd} has a high influence on the critical load. This parameter is estimated with the results of analysis to boundary imperfections from Knebel (1997). A critical amplitude of the boundary imperfection $u^a_{0,\text{bd}}(y)$ (controlled by a_{bd}) is about 0.01 mm, where the critical buckling load decreases rapidly. Especially for this parameter, more measurements are needed. Therefore, a large interval and no fuzzy variable is defined.

5.3 | Uncertainty models for material and thickness imperfections

In Delft's imperfection data bank (Arbocz & Abramovich, 1979), experimental results are given for Young's modulus E and shell thickness t of the seven A-shells, see Table 4. No information for E and t to spatial variation is known and therefore no akfs can be constructed. Especially the measurement of the spatial variation of the material parameters is extremely difficult. However, seven measurements are enough to define a fuzzy variable of each parameter. For this purpose, the measured values are displayed in a histogram. The defined membership function and the histogram of both parameters are depicted in Figure 18.

The minimum and maximum measured Young's modulus and thickness are defined as the left and right limits of the support of the fuzzy variable. The trend value represents the mean value of the measurements. The fuzzy triangular numbers are defined as follows:

$$\begin{aligned} \tilde{E} &= \langle 101350,\ 104406,\ 108940 \rangle \quad (\text{N/mm}^2) \\ \tilde{t} &= \langle 0.111,\ 0.116,\ 0.1204 \rangle \quad (\text{mm}) \end{aligned} \tag{35}$$

A relative strict definition is made for both parameters. It is assumed that it is easier to specify tolerances for the Young's modulus and shell thickness than for the correlation parameters, which are more difficult to obtain. Therefore, no membership is assigned to the values outside the range of the measured values.

5.4 | Discussion to uncertainty quantification of shell imperfections

In summary, all chosen uncertainty models for shell imperfections are shown in Table 5. All uncertainties of different shell imperfections are quantified with suitable uncertainty models based on the available data. The concept of polymorphic uncertainty modeling allows the explicit distinction between aleatoric and epistemic uncertainties in modeling of shell imperfections. For example, the available data for surface imperfections allow a modeling with fp-rfs. There are not enough data available for classical modeling with random fields. To determine one specific correlation length is very brave if the variations of the akfs are observed in Figure 11.

The epistemic component of the correlation parameters has to be taken into account in order to avoid false assumptions. On the other hand, only one measurement for boundary imperfections is available. The definition of a fuzzy variable with only one measured value and no available expert knowledge is not possible and would feign a nonexistent knowledge to the parameter. Therefore, intervals are chosen to model boundary imperfections with an ip-rf. For the material and thickness imperfections, no data to spatial variability are available. Thus, a random field modeling is not possible. However, seven measurements are enough to evaluate the data to define a fuzzy variable for the Young's modulus and shell thickness. The ability to choose an uncertainty model based on available data is the essential benefit of the introduced concept. This

TABLE 5 Overview of polymorphic uncertainty models used for different shell imperfections.

Imperfection form	Uncertainty model	Data & characteristic	Notes to the choice
Surface imperfections	Fuzzy probability–based random field (fp-rf) $\tilde{\sigma}^2 = \langle 0.002,\ 0.007,\ 0.012 \rangle$ $\tilde{\ell}_{c,h} = \langle 2000,\ 9000,\ 13000 \rangle$ $\tilde{\ell}_{c,u} = \langle 175,\ 225,\ 400 \rangle$	Aleatoric & epistemic, few data, Gaussian random field and a correlation model with uncertain data: $\tilde{C}(\tau) = \tilde{\sigma}^2\ \tilde{\rho}(\Delta x)\ \tilde{\rho}(\Delta y)$	Conservative choice of parameters due to limited expert knowledge of correlation properties
Boundary imperfections	Interval probability–based random field (ip-rf) $T_{\mathrm{bd}} \in [100,\ 500]$ $a_{\mathrm{bd}} \in [10,\ 20]$ $\ell_{c,\mathrm{bd}} = 494$	Aleatoric & epistemic, few unvaluable data, Gaussian random field and a correlation model with uncertain data: $C(\Delta y) = \sigma^2 \rho(\Delta y, \ell_{c,\mathrm{bd}}, T_{\mathrm{bd}})$	Only one measurement available, too little data basis for an evaluation, no information about the imperfection amplitude
Material imperfections	Fuzzy variable $\tilde{E} = \langle 101350,\ 104406,\ 108940 \rangle$	Epistemic, few data, an evaluation of the data is possible	Correlation properties for random field modeling are unknown
Thickness imperfections	Fuzzy variable $\tilde{t} = \langle 0.111,\ 0.116,\ 0.1204 \rangle$	Epistemic, few data, an evaluation of the data is possible	Correlation properties for random field modeling are unknown

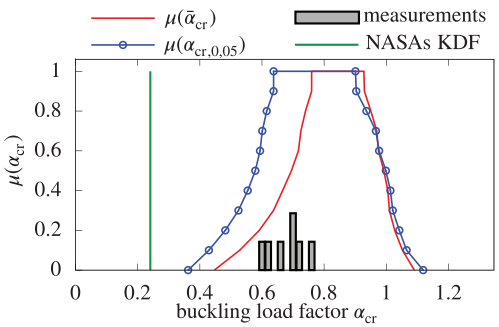

FIGURE 19 Results of the buckling analysis with polymorphic uncertain parameters.

avoids generating false assumptions and leads to a more truthful modeling.

5.5 | Numerical results

The results of the buckling analysis with polymorphic uncertain parameters from Table 5 are depicted in Figure 19.

According Equation (28), all buckling loads P_{cr} are normalized by the critical load $P_{cr,\mathrm{perf}} = 5073$ N. Overall, seven input parameters are defined

$$\tilde{\boldsymbol{s}} = \{\tilde{\sigma}^2,\ \tilde{\ell}_{c,h},\ \tilde{\ell}_{c,u},\ T_{\mathrm{bd}},\ a_{\mathrm{bd}},\ \tilde{E},\ \tilde{t}\} \tag{36}$$

In order to reduce the computational effort, a surrogate model based on the HDMR of second order and LS polynomial approximation is used. Therefore, on 365 points of the input space, a MCS with 500 realizations has to be performed to get sufficiently accurate results. This means $365 \times 500 = 182,500$ buckling analyses are performed. The critical buckling load factor is an fp-r variable. Thereof, the membership functions of the fuzzy mean value $\bar{\alpha}_{\mathrm{cr}}$ and the fuzzy 5% quantile $\alpha_{\mathrm{cr},0.05}$ are depicted in Figure 19. In addition, the experimental results of the buckling load factors of the seven investigated shells and NASA's KDF are also shown in Figure 19. The histogram of the experimental results is in the range of the highest membership $\mu = 1$, which is an indication of appropriate uncertainty quantification. The KDF amounts to $\alpha_{\mathrm{cr}} = 0.24$ and is significantly smaller than the left boundary of the resulted membership functions. Thus, it can be shown that the KDF as a representation for traditional design concepts is very conservative. The results show that there is much potential to specify higher buckling load factors as the basis of a shell design. This means a more economical design is possible. As a first idea, Figure 20 depicts an alternative safety concept.

There, the result membership function of the fuzzy 5% quantile $\alpha_{\mathrm{cr},0.05}$ is overlaid with a safety level based on nonpermissible buckling load factors defined with a fuzzy variable. The advantage of such a fuzzy-valued safety level is that verbal statements can be considered. Here, verbal statements to imperfection sensitivity are given. For example, low buckling load factors indicate a high imperfection sensitive structure. The overlap area of the result variable and a defined fuzzy-valued safety level represents a kind of danger of buckling. This area can be used as a design parameter. How much overlapped area can be permitted must be discussed in further works.

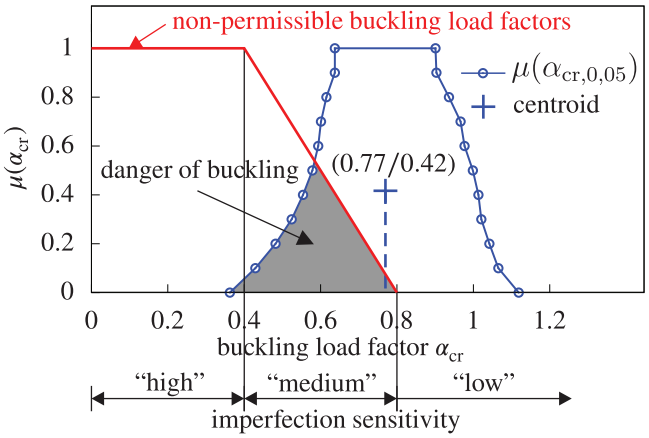

FIGURE 20 Definition of a danger of buckling for an alternative safety concept.

6 | CONCLUSIONS

In the presented contribution, the concept of polymorphic uncertainties to consider aleatoric and epistemic uncertainties is introduced in shell buckling. The choice of suitable uncertainty models based on available data for different imperfection types such as surface, boundary, material, and thickness imperfections is discussed in detail. It should be emphasized that the choice is based on the available data. This avoids generating false assumptions and leads to a more truthful modeling. This should open up new perspectives moving away from deterministic thinking in civil and other engineering disciplines. Therefore, an approach for a new design concept with a fuzzy-valued safety level is formulated. Based on verbal statements to the imperfection sensitivity, nonpermissible buckling load factors are defined. An overlap area with the result variable represents a kind of danger of buckling. The presented approach allows to consider different verbal statements, for example, to financial, social, or hazard potential to life. Finally, the concept has to be applied for composite structures, which provide a wide and interesting research field.

ACKNOWLEDGMENTS

Open access funding enabled and organized by Projekt DEAL.

CONFLICT OF INTEREST STATEMENT

The authors declare no potential conflict of interests.

ORCID

Marc Fina https://orcid.org/0000-0002-6956-6112

REFERENCES

Arbocz, J. (2000). The effect of imperfect boundary conditions on the collapse behavior of anisotropic shells. *International Journal of Solids and Structures*, *37*(46), 6891–6915.

Arbocz, J., & Abramovich, H. (1979). *The initial imperfection data bank at the Delft University of Technology: Part I*. Faculty of Aerospace Engineering. Tech. rep.

Beer, M. (2002). *Fuzziness und Fuzzy-Zufälligkeit bei der Sicherheitsbeurteilung von Tragwerken. H.5*. Lehrstuhl für Statik, TU Dresden.

Beer, M., Ferson, S., & Kreinovich, V. (2013). Imprecise probabilities in engineering analyses. *Mechanical Systems and Signal Processing*, *37*(1), 4–29.

Broggi, M., & Schuëller, G. (2011). Efficient modeling of imperfections for buckling analysis of composite cylindrical shells. *Engineering Structures*, *33*(5), 1796–1806.

Ditlevsen, O. (1982). Extended second moment algebra as an efficient tool in structural reliability. *Nuclear Engineering and Design*, *71*(3), 317–323.

Ditlevsen, O., & Munch-Andersen, J. (1995). Empirical stochastic silo load model. I: Correlation theory. *Journal of Engineering Mechanics*, *121*(9), 973–980.

Dubois, D., & Prade, H. (1988). *Possibility theory: An approach to computerized processing of uncertainty*. Plenum Press.

Faes, M., Daub, M., Marelli, S., Patelli, E., & Beer, M. (2021). Engineering analysis with probability boxes: A review on computational methods. *Structural Safety*, *93*, 102092.

Faes, M., & Moens, D. (2019). Recent trends in the modeling and quantification of non-probabilistic uncertainty. *Archives of Computational Methods in Engineering*, *27*(3), 633–671.

Fina, M. (2020). *Polymorphe Unschärfemodellierung in der nichtlinearen Strukturmechanik – Stabilität von Schalentragwerken, räumliche Variabilität und Metamodellierung*. B. 27, Institut für Baustatik, KIT.

Fina, M., Panther, L., Weber, P., & Wagner, W. (2021). Shell buckling with polymorphic uncertain surface imperfections and sensitivity analysis. *ASCE-ASME Journal of Risk and Uncertainty in Engineering Systems Part B: Mechanical Engineering*, *7*(2), 020909.

Fina, M., Weber, P., & Wagner, W. (2019a). A fuzzy stochastic correlation model for geometric imperfections of cylindrical shells. In *13th international conference on applications of statistics and probability in civil engineering (ICASP13)*. May 26-30, 2019, Seoul.

Fina, M., Weber, P., & Wagner, W. (2019b). Modeling of aleatory and epistemic uncertainties in probabilistic design of cylindrical shells. In M. Beer, & E. Zio (Eds.) *Proceedings of the 29th European safety and reliability conference (ESREL)*. Research Publishing, September 22-26, Hannover, Germany.

Fina, M., Weber, P., & Wagner, W. (2020). Polymorphic uncertainty modeling for the simulation of geometric imperfections in probabilistic design of cylindrical shells. *Structural Safety*, *82*, 101894.

Freitag, S., Edler, P., Kremer, K., Hofmann, M., & Meschke, G. (2018). Optimization approaches for durable reinforced concrete structures considering interval and stochastic parameter uncertainty. *PAMM*, *18*(1), e201800444.

Graf, W., Götz, M., & Kaliske, M. (2014). Structural design with polymorphic uncertainty models. In M. Modares (Ed.) *6th international conference on reliable engineering computing*. 64–76, May 25-28, 2014, Chicago, USA.

Graf, W., Götz, M., & Kaliske, M. (2015). Analysis of dynamical processes under consideration of polymorphic uncertainty. *Structural Safety*, *52*, 194–201.

Górski, J., Mikulski, T., Oziębło, M., & Winkelmann, K. (2015). Effect of geometric imperfections on aluminium silo capacities. *Stahlbau*, *84*(1), 52–57.

Gruttmann, F., & Wagner, W. (2006). Structural analysis of composite laminates using a mixed hybrid shell element. *Computational Mechanics*, (37), 479–497.

Götz, M. (2017). *Numerische Entwurfsmethoden unter Berücksichtigung polymorpher Unschärfe – Aspekte zeitlicher und räumlicher Abhängigkeiten*. H.32. Institut für Statik und Dynamik der Tragwerke, TU Dresden.

Hilburger, M. (2012). Developing the next generation shell buckling design factors and technologies. In *53rd AIAA/ASME/ASCE/AHS/ASC structures, structural dynamics and materials conference*. April 23-26, 2012, Honolulu, Hawaii.

Javidan, M. M., & Kim, J. (2022). Fuzzy-based method for efficient seismic performance evaluation of structures with uncertainty. *Computer-Aided Civil and Infrastructure Engineering*, *37*(6), 781–802.

Klompé, A., & den Reyer, P. (1989). *The initial imperfection data bank at the Delft University of Technology: Part III*. Faculty of Aerospace Engineering. Tech. rep.

Knebel, K. (1997). *Stabilität von Stahlzylindern mit unilateralen Randbedingungen bei statischen und dynamischen Beanspruchungen*. B. 17.2, Institut für Baustatik, Universität Karlsruhe (TH).

Lauterbach, S., Fina, M., & Wagner, W. (2018). Influence of stochastic geometric imperfections on the load-carrying behaviour of thin-walled structures using constrained random fields. *Computational Mechanics*, *62*(5), 1107–1125.

Li, C., & Kiureghian, A. (1993). Optimal discretization of random fields. *Journal of Engineering Mechanics*, *119*(6), 1136–1154.

Liang, Y.-P., Feng, D.-C., Ren, X., & Li, J. (2022). Three-stage non-Gaussian homogeneous random field representation over manifolds. *Computer-Aided Civil and Infrastructure Engineering*, 1–21.

Möller, B., & Beer, M. (2004). *Fuzzy randomness—Uncertainty in civil engineering and computational mechanics*. Springer.

Möller, B., & Beer, M. (2008). Engineering computation under uncertainty—apabilities of non-traditional models. *Computers & Structures*, *86*(10), 1024–1041.

Möller, B., Graf, W., & Beer, M. (2000). Fuzzy structural analysis using α-level optimization. *Computational Mechanics*, *26*(6), 547–565.

Pannier, S., Waurick, M., Graf, W., & Kaliske, M. (2013). Solutions to problems with imprecise data—An engineering perspective to generalized uncertainty models. *Mechanical Systems and Signal Processing*, *37*(1), 105–120.

Rabitz, H., & Aliş, Ö. F. (1999). General foundations of high-dimensional model representations. *Journal of Mathematical Chemistry*, *25*(2), 197–233.

Reuter, U. (2013). Ungewissheit im Bauingenieurwesen–Spezifikation, Modellierung und Berechnung. In S. Jeschke, E.-M. Jakobs, & A. Dröge (Eds.) *Exploring uncertainty* (pp. 179–208). Springer.

Schenk, C., & Schuëller, G. (2003). Buckling analysis of cylindrical shells with random geometric imperfections. *International Journal of Non-Linear Mechanics*, *38*(7), 1119–1132.

Schietzold, F., Graf, W., & Kaliske, M. (2021). Multi-objective optimization of tree trunk axes in glulam beam design considering fuzzy probability based random fields. *ASCE-ASME Journal of Risk and Uncertainty in Engineering Systems Part B: Mechanical Engineering*, *7*(2), 020913.

Schietzold, F., Schmidt, A., Dannert, M., Fau, A., Fleury, R., Graf, W., Kaliske, M., Könke, C., Lahmer, T., & Nackenhorst, U. (2019). Development of fuzzy probability based random fields for the numerical structural design. *Special Issue: Polymorphic Uncertainty Modelling for Numerical Design of Structures—Part I, GAMM - Mitteilungen*, *42*(1), e201900004.

Sienz, J. (1992). *Nege reference manual*. Department of Civil Engineering, University of Wales Swansea.

Sudret, B., & Kiureghian, A. (2000). *Stochastic finite element methods and reliability—A state-of-the-art report*. Tech. rep., Department of Civil & Environmental Engineering University of Calfifornia, Berkeley.

Taylor, R. L. (2023). *Finite element analysis program (FEAP)*. http://www.ce.berkeley.edu/projects/feap/

Timoshenko, S., & Gere, J. (1961). *Theory of elastic stability*. Dover Publications, Inc.

Vanmarcke, E. (2010). *Random fields: Analysis and synthesis*. World Scientific.

Wagner, H., Hühne, C., & Elishakoff, I. (2020). Probabilistic and deterministic lower-bound design benchmarks for cylindrical shells under axial compression. *Thin-Walled Structures*, *146*, 106451.

Wagner, W., & Gruttmann, F. (2005). A robust non-linear mixed hybrid quadrilateral shell element. *International Journal for Numerical Methods in Engineering*, *64*(5), 635–666.

Wagner, W., & Wriggers, P. (1988). A simple method for the calculation of postcritical branches. *Engineering Computations*, *5*(2), 103–109.

Wang, J., Liu, X.-Z., & Ni, Y.-Q. (2018). A Bayesian probabilistic approach for acoustic emission-based rail condition assessment. *Computer-Aided Civil and Infrastructure Engineering*, *33*(1), 21–34.

Weber, P., Fina, M., & Wagner, W. (2019). Time domain simulation of earthquake exited buildings using a fuzzy stochastic approach. In M. Beer, & E. Zio (Eds.) *Proceedings of the 29th European safety and reliability conference (ESREL)*. Research Publishing, September 22-26, Hannover, Germany.

Weingarten, V., & Seide, P. (1968). *Buckling of thin-walled truncated cones*. Tech. rep., NASA.

Zadeh, L. (1965). Fuzzy sets. *Information and Control*, *8*(3), 338–353.

How to cite this article: Fina, M., Wagner, W., & Graf, W. (2023). On polymorphic uncertainty modeling in shell buckling. *Computer-Aided Civil and Infrastructure Engineering*, 1–16. https://doi.org/10.1111/mice.13054